SCIENTIFIC REPORTS

OPEN

SUBJECT AREAS:
NANOPARTICLES
MOLECULAR SELF-ASSEMBLY

Received
22 May 2014

Accepted
24 September 2014

Published
23 October 2014

Correspondence and requests for materials should be addressed to T.H. (th358@cornell.edu)

Connecting the Particles in the Box - Controlled Fusion of Hexamer Nanocrystal Clusters within an AB_6 Binary Nanocrystal Superlattice

Benjamin E. Treml[1], Binit Lukose[2], Paulette Clancy[2], Detlef-M Smilgies[3] & Tobias Hanrath[2]

[1]Department of Materials Science & Engineering, Cornell University, Ithaca NY 14853, [2]School of Chemical & Biomolecular Engineering, Cornell University, Ithaca NY 14853, [3]Cornell High Energy Synchrotron Source, Cornell University, Ithaca NY 14853.

Binary nanocrystal superlattices present unique opportunities to create novel interconnected nanostructures by partial fusion of specific components of the superlattice. Here, we demonstrate the binary AB_6 superlattice of PbSe and Fe_2O_3 nanocrystals as a model system to transform the central hexamer of PbSe nanocrystals into a single fused particle. We present detailed structural analysis of the superlattices by combining high-resolution X-ray scattering and electron microscopy. Molecular dynamics simulations show optimum separation of nanocrystals in agreement with the experiment and provide insights into the molecular configuration of surface ligands. We describe the concept of nanocrystal superlattices as a versatile 'nanoreactor' to create and study novel materials based on precisely defined size, composition and structure of nanocrystals into a mesostructured cluster. We demonstrate 'controlled fusion' of nanocrystals in the clusters in reactions initiated by thermal treatment and pulsed laser annealing.

New opportunities to create materials with properties by design continue to emerge from advances in our ability to control structure and composition of nanomaterials through wet-chemistry methodologies. Access to nanomaterial building blocks with precisely programmable size, shape, and composition has provided critical insights into our understanding of and control over fundamental structure-property relationships. At the same time, prototype nanomaterials have enabled rapid advances in nanotechnology underscored by their immense technological potential in a broad range of applications ranging from photovoltaics[1–3], catalysis[4,5], energy storage[6], and thermoelectrics[7]. Focus in the field is now shifting towards controlling the interactions among nanocrystals (NCs), driven by the desire to create programmable and purposeful connections between NCs and their surrounding in ordered assemblies.

Binary assemblies of NCs[8] with dissimilar properties have drawn particular interest as a model structure for designer metamaterials in which controlled interactions between component NCs lead to magneotoresistance[9], catalytic activity[10], and conductivity[11] greater than the sum of the constituent parts.

Moreover, binary NC superlattices (BNSLs) provide a versatile experimental test bed to study clusters of NCs in confined volumes. The AB_6 superlattice, consisting of type A particles at the corners of the unit cell and a B_6 hexamer in the center position, presents a particularly interesting example. Previous studies have shown that the complete description of the interactions among NCs assembling into superlattices must go beyond the approximation of spherical or polyhedral particles[12,13]. To satisfactorily explain the self-assembly behavior of NCs, the molecular-level interactions of ligands bound to the NC surface and electrostatic interactions must be considered. In the specific case of the AB_6 structure, this introduces questions about the orientational alignment of the polyhedral NCs and the configuration of the ligands in the confined volume of the central hexamer.

Understanding and controlling the arrangement of NCs within isolated clusters also presents opportunities to create novel metamaterials *via* selective fusion of one component of the superlattice. '*Connecting the dots*' in the cluster can be achieved by either chemical treatments (*i.e.*, exchanging or displacing the native long-chain ligands[14]) or physical treatments (*i.e.* compression[15] or thermal annealing[16]). During thermal annealing, single component assemblies are susceptible towards fusion[16,17]. On the other hand, NCs isolated in a binary lattice have been demonstrated to be robust to coalescence[10]. The structural evolution of the central hexamer of an AB_6 BNSL has, to the best of our knowledge, not yet been investigated.

In this work, we use BNSLs with the AB_6 structure as a self-assembled periodic "nanoreactor." A framework of Fe_2O_3 NCs confine a cluster of six PbSe NCs, allowing us to study the interactions among a specific number of particles assembled in the center of the superlattice unit cell. The integration of synchrotron-based X-ray scattering and computational simulation probes the structure of the BNSL at unprecedented level of detail. We show how the periodic nature of the BNSL can be leveraged to study structure transformations by applying grazing incidence small angle X-ray scattering (GISAXS) and investigate a large number ($\sim 10^{10}$) of nanoreactors simultaneously. We demonstrate how PbSe NCs in the central hexamer are transformed into a single particle *via* thermal annealing and how the progress of the nanoreaction can be rationally controlled by changing the time scale of heating *via* laser spike annealing. We show that BNSLs are not only a novel class of metamaterials with promising properties, but also can serve as a powerful tool to study the interparticle interactions of precisely defined numbers of NCs.

Results

We characterized the structure of the self-assembled BNSL using a suite of microscopy and scattering techniques. Analysis of samples prepared on TEM grids confirmed the assembled structure as an AB_6 (A = Fe_2O_3, B = PbSe, $Pm\bar{3}m$ no. 221) structure comprised of a simple cubic lattice of 13.4 nm Fe_2O_3 NCs with six 4.2 nm PbSe NCs occupying the center of the unit cell. The central hexamer is structurally analogous to the arrangement of NCs in a unit cell of a body-centered tetragonal assembly. Transmission electron micrographs of the assembled BNSLs in Figures 1a and 1c show the structure of the Fe_2O_3 and PbSe NCs, respectively. Superlattice grains in the optical micrograph display square faceting concomitant with the cubic unit cell of the BNSL.

GISAXS characterization of assembled BNSLs. GISAXS provides detailed, unbiased insights into the structure of the BNSL averaged over as many as 10^{10} unit cells. GISAXS corroborates microscopic structure analysis, and adds additional information that would be impractical or impossible to obtain from electron microscopy alone. A typical GISAXS pattern is shown in Figure 1d. Along the horizontal axis GISAXS probes the density correlation among nanoparticles in the substrate plane; in the vertical direction density correlations perpendicular to the substrate surface are probed. Analysis of the location of scattering peaks indicates that the BNSL has a simple cubic lattice oriented with the (001) plane parallel to the substrate and a lattice constant of 17 nm. In addition, the width of the peaks can be used to determine the average supercrystal grain size by extending the Scherrer equation to GISAXS[18]. The scattering patterns give a lower bound of 81 nm for supercrystal thickness, and 186 nm for in plane size. Due to instrument resolution, only lower bounds can be established as many of the scattering peaks were near the instrumental broadening for the GISAXS setup used.

Large superlattices with a high degree of preferential orientation give rise to high quality scattering patterns with many well-resolved, intense peaks. As a result, we could extend the treatment of GISAXS developed in previous studies[19] to binary assemblies, and focus on the intensity of the GISAXS peaks to study the internal structure of the unit cell. Simulations of GISAXS have used the quasi-kinematic approximation to produce simulated scattering patterns and quantify NC film order[19,20]. Within this approach, the scattering from a NC assembly can be split into contributions from the form factor of the individual NCs and the structure factor of the assembly. The scattering from spheroidal NC can be approximated by the hard sphere form factor[21,22]:

$$f(q) = \frac{4}{3}\pi R^3 \rho \left[3\frac{\sin(qR) - qR\cos(qR)}{(qR)^3} \right] \quad (1)$$

where q is the magnitude of the scattering vector, R is the particle radius, and ρ is the electron density of the material. The calculated form factors used in further calculations are averaged over a population with mean size and standard deviation determined from TEM measurements of at least 100 particles.

The scattering peaks observed in GISAXS patterns are a result of the structure factor of the superlattice. The structure factor is calculated as:

$$S(\mathbf{q}_{hkl}) = \sum_n f_n(\mathbf{q}_{hkl}) \exp[2\pi i(hx_n + ky_n + lz_n)] \quad (2)$$

where $\mathbf{q}_{hkl}$ is the scattering vector for the *hkl* reflection, and $x_n\ y_n\ z_n$ are the fractional coordinates of the nth NC in the unit cell. We chose that for n = 1, a Fe_2O_3 NC is located at 0,0,0 and, for n = 2 through 7, six PbSe NCs are located at permutations of ½, ½, X and ½, ½, 1-X. Our computational model of the scattering intensity systematically varies X to change the interparticle spacing between the PbSe NCs which is 1-2X in the [001] direction.

Lastly, we add a Debye-Waller factor, *B*, to model disorder of the first kind, which involves local deviation from ideal lattice sites without disrupting the long-range order of the supercrystal. The effect of

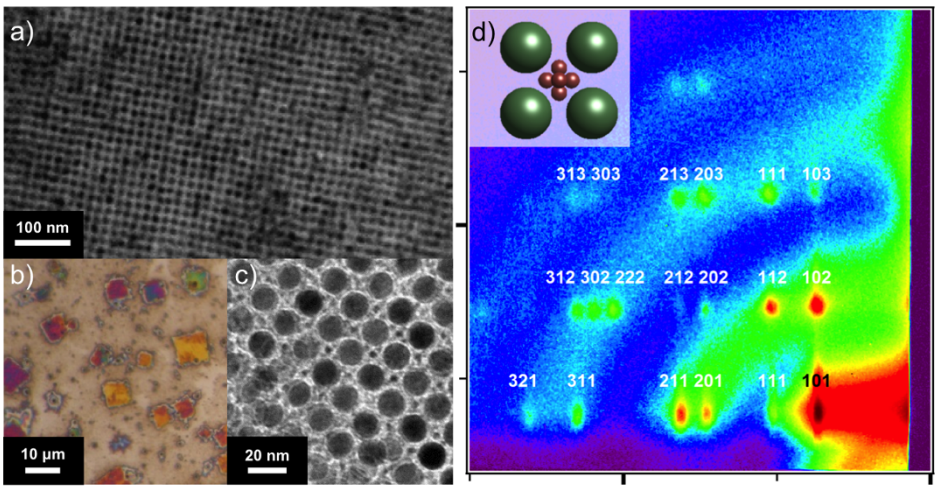

Figure 1 | Characterization of the assembled BNSL. (a) Low magnification TEM of a BNSL showing long-range ordering of the Fe_2O_3 NCs. (b) Optical micrograph of BNSL assembled on a Si wafer. (c) Higher magnification TEM showing the structure of the hexamer (d) Indexed GISAXS scattering pattern of the BNSL. Intensity shown on a logarithmic scale. Bold ticks indicate 1 nm^{-1} Inset: Model of the 001 projection of the assembled AB_6 BNSL.

the Debye-Waller factor on scattering is taken into account by W:

$$W(q) = \exp\left(-B^2 q^2\right) \quad (3)$$

and is used to give the correct weight to structure and form factors in the calculations. The final intensities are then calculated from[22]:

$$\mathrm{I(q)} \propto \mathrm{S(q)^2 * W(q)} + \left(\sum_{\mathrm{n}} \mathrm{f_n}(q)\right)^2 * (1 - \mathrm{W(q)}) \quad (4)$$

The large number of scattering peaks (over 15) resolved in our GISAXS analysis of the AB_6 BNSLs presented an opportunity to study the superlattice structure at an unprecedented level of detail. To match experimental and simulated scattering patterns, the intensity of nine peaks common to scattering patterns of interest and of reliable intensity were analyzed for a variety of locations of the PbSe NCs (*i.e.*, X detailed above) in the BNSL unit cell. We optimized the unit cell configuration of the model structure based on the lowest sum of squared residuals. The residual from each peak was weighed by a factor of q^4 to account for the asymptotic q^{-4} decrease in form factor as given by Porod's Law[22]:

$$r_{hkl} = q_{hkl}^4 (I_{obs} - I_{calc}) \quad (5)$$

This choice of residual makes the structure simulation more sensitive to the structure factor information in the weak reflections at higher q, which otherwise would barely contribute to the fit. Comparison of simulated and experimental scattering intensities allowed us to precisely determine the location of the PbSe NCs in the unit cell. The structure of the confined hexamer NCs is an octahedron with side lengths of 4.7 nm and a tip-to-tip distance of 6.6 nm. The tips of the octahedron are oriented towards the center of the faces of the cube formed by the iron oxide particles. Importantly, we found that face-to-face spacing between quasi-spherical PbSe NCs is only 0.5 nm, which is significantly less than the interparticle spacings previously reported in pure PbSe NC superlattices[23]. The tight interparticle spacing in the center hexamer introduces an interesting question: *What is the molecular configuration of the ca. 1.8 nm long oleic acid ligand in the confined cavity of the PbS hexamer?* To obtain a deeper understanding of the molecular configuration of the ligands in the center hexamer, we turn to Molecular Dynamics simulations detailed below.

Molecular Dynamics Simulations. MD simulations provide insight into the disposition of the oleic acid ligands and the extent of ligand coverage which are difficult to probe experimentally. We used a coarse-grained model to represent the intramolecular potentials; this model treats CH_x groups in the ligands as united atoms (UA), *i.e.*, as single "beads" on the oleic acid backbone. Kaushik *et al.*[13] studied the self-assembly of PbSe nanocrystals with similar ligands, adopting the model developed by Paul *et al.*[24] for the coarse-graining to avoid spurious ligand aggregation effects. We have adopted the same model and parameters for our study. The intermolecular interactions between NCs, ligands and NC-ligand pairs were modeled by (12-6) Lennard-Jones potential between UAs; Lorentz-Berthelot mixing rules were applied to describe the interaction between dissimilar UAs.

Consistent with TEM images, we modeled the Fe_2O_3 NCs as simple spheres. The detailed shape of the PbSe NCs in the hexamer is interesting and merits further discussion. Using the detailed experimental structure parameters as inputs to the model, we can infer the shape of the PbSe NCs to be a truncated octahedron. Truncated-cube and cuboctahedra shapes on the other hand can be ruled out since these polyhedral cannot be arranged, without overlap, into the hexamer with interparticle spacings as determined from our experimental data. Detailed aspects of the MD model are provided in the supporting information.

MD simulations provide insight into an aspect of BNSL assemblies that is experimentally unavailable and is, to the best of our knowledge, previously unexplored, namely, how oleic acid ligands adapt to the inhomogeneous local environment of a BNSL. The structure of the hexamer contains two types of cavities between PbSe NCs into which ligands can expand: one *interior* cavity in the center of the hexamer and eight *exterior* cavities between the PbSe NCs and the surrounding Fe_2O_3. The ligands are largely interdigitated in the inner cavity; however, those in the outer cavities are projected towards the Fe_2O_3 NCs. To unravel the preferred orientation of NCs covered with oleic acid ligands in the hexamer, we applied steered molecular dynamics (SMD) on six NCs displaced from a common point along six axes. We have considered multiple initial orientations to allow NCs to orient differently and hence remove bias in the results from our initial guess.

We systematically varied the PbSe NC ligand coverage to create a model of the hexamer with inter-NC separation consistent with the experimentally determined spacing. The van der Waals energy plot in Figure 2c shows the correlation between interparticle spacing and ligand coverage; this relationship implies that the PbSe NC surface ligand coverage density in the experimental system is slightly less than 1 nm^{-2}. The results indicate that the ligands in a PbS hexamer can adapt to an interparticle spacing closer than has been observed in single component assemblies when there is additional free space in the assembly into which the ligands can expand. Moreover, these simulations show that the depth of the potential energy well for the central hexamer correlates directly to the ligand coverage; this trend suggests that NC rearrangement in the hexamer with sparse ligand coverage requires less energy compared to rearrangements of NCs in conventional assemblies with denser ligand coverage.

Structural Transformation of the PbS hexamer and the BNSL during thermal annealing. Experimental and computational insights into the structure of the hexamer introduce the interesting prospect of controllably fusing the six particles into a single fused NC cluster. The structural analysis detailed above illustrates that the BNSL effectively confines a single hexamer unit cell of PbSe NC in a periodic manner. This confinement opens several possibilities to process the hexamer and transform the particles-in-a-box to novel clusters with programmable structures. The conventional approach to form connections between colloidal NCs involves chemical treatments such as ligand removal or exchange[14,25,26]; however, efficient mass transport of ligands both into and out of the BNSL presents a significant challenge. Moreover, chemical ligand treatments would not be specific to the hexamer since the treatment would displace ligands from the hexamer as well as from the confining Fe_2O_3 NC framework. Thermal annealing on the other hand presents an opportunity to mitigate the transport limitation as well as selective treatment of one of the components of the binary lattice. The BNSLs contain components with both high (Fe_2O_3) and low (PbSe) thermal stability. The higher melting point of the metal-oxide NCs therefore provides a stable non-reactive framework that keeps individual hexamers separated.

Melting and sintering of NCs involves an intricate interplay of thermodynamic and kinetic aspects[16,27,28] that can lead to complicated structural rearrangements[17]. We hypothesized that controlling the temperature and duration of thermal annealing will allow us to decouple the thermodynamic and kinetic aspects and rationally program the resulting NC structures. Figure 3 illustrates three potential outcomes of structures resulting from thermal annealing of an AB_6 superlattice. The initial as-assembled superlattice structure in the upper left quadrant can be transformed by either, partial sintering inward, partial sintering outward, and complete sintering inward of the NCs.

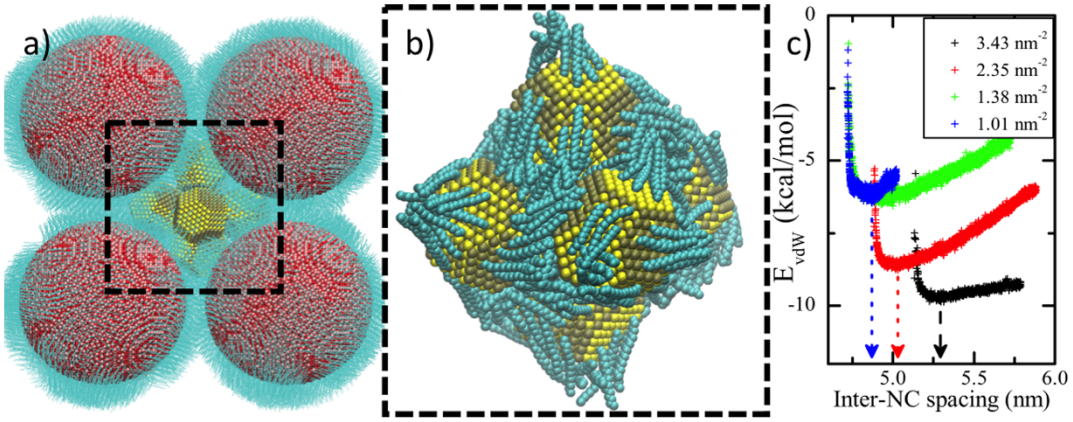

Figure 2 | Molecular Dynamics snapshots of the system. (a) BNSL formed by Fe_2O_3 spheres (red) and six PbSe NC (yellow) that define the hexamer. (b) Snapshot of the NC orientation and molecular configuration of ligands in a hexamer with a surface ligand density of 1.1 nm^{-2}. The ligand density is 1.1 nm^{-2}. The coarse-grained UA ligands (turquoise) in the inner cavity are largely interdigitated. Atoms are shown as van der Waals spheres. (c) van der Waals potential energy as a function of inter-NC distance illustrates the relationship between equilibrium spacing and ligand coverage.

To understand the structural evolution of the PbSe hexamer during thermal annealing, we analyzed GISAXS patterns *in situ* while heating the sample from 30°C to near 200°C. Similar *in-situ* experiments previously revealed the structure evolution during annealing of a single component NC superlattice[16]. An attractive aspect of studying structure transitions in an AB_6 BSNL is that we can focus on the specific fusion of a fixed number of NCs (*i.e.*, six PbSe NCs in the central hexamer). We provide a movie illustrating the evolution of the scattering patterns with temperature in the supplementary information. The *in situ* experiment reveals a gradual loss of peaks at high q-values. This trend can be attributed to disorder in the superlattice, and is quantified by the Debye-Waller factor included in our calculated GISAXS intensities. Moreover, changes in the relative intensities of the scattering peaks (*i.e.*, (201) and (211), and (103) and (113) reflections) provide an advantageous scattering fingerprint to monitor the evolution of the BSNL structure; these peaks are highlighted in Figure 4b. For both pairs of scattering peaks the ratio of intensities, $\frac{I_{201}}{I_{211}}$ and $\frac{I_{103}}{I_{113}}$, is initially > 1 and becomes < 1 over the course of the annealing. Since the peaks are at nearly the same q value, the change in relative intensities cannot be attributed to Debye-Waller disorder. Instead, the changing intensities indicate a change in the structure factor, and hence changes in the interior structure of the unit cell.

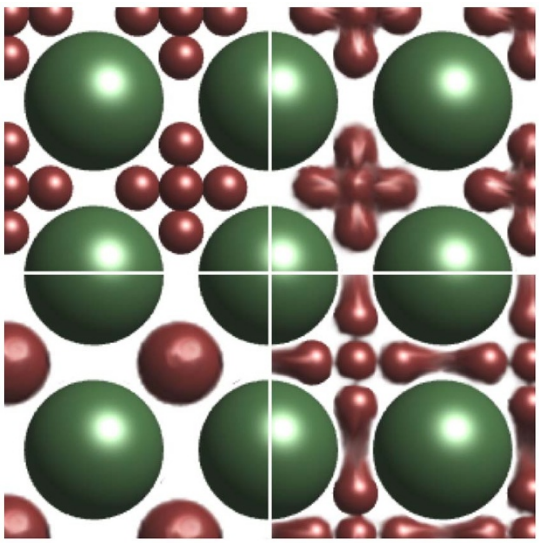

Figure 3 | Possible outcomes of annealing the hexamer of PbSe particles (red) confined by a periodic arrangement of the Fe_2O_3 particles (green).

We carefully monitored the structural evolution of the PbSe hexamer throughout the *in situ* experiment, by comparing the intensities of scattering peaks at a given temperature to the simulated intensities corresponding to a range of interparticle spacings and hypothesized structural transformations. Our simulations of the scattering patterns suggest that the hexamer of PbSe NCs in the center of the initial AB_6 superlattice structure is transformed into a superstructure with a single central PbSe particle. The residuals of the scattering fits plotted in Figure 4a show the best fit for a hexamer with distinct particles at temperatures up to 125°C whereas the sample annealed to 140°C indicates a fused structure. We modeled the fused structure as either a single 7.6 nm NC or six overlapping NCs. The residual for the fit for both structures is similar so a definitive assignment of the fused structure to a single spherical particle or fused hexamer with octahedral shape is not feasible from analysis of X-ray scattering data alone. Additional high-resolution electron microscopy and tomography are required to gain deeper insights into the detailed three-dimensional structure of the fused hexamer. In the case of conventional thermal annealing, the shift from separate to fused particles occurs near a temperature of 130°C without any apparent transition through intermediate configurations. This can be understood by considering the structure of the hexamer at the intermediate stage between separated and fused. As particles move inward, they eventually come into contact and form a neck between previously separated NCs. The particles then quickly sinter either via plastic deformation or surface diffusion of atoms to minimize the surface energy of the NCs, resulting in complete fusion of the particles[29,30].

The observed transition temperature is consistent with temperatures at which rotation and fusion of PbSe NCs was previously reported from *in situ* TEM experiments[29], as well as the temperature for the order-disorder transition in single component PbSe NC superlattices[16]. We further corroborated the results of our *in situ* experiment by annealing BNSLs assembled on TEM grids. Figure 4e shows that PbSe NCs have fused while remaining separate from the NCs in adjacent unit cells, indicating that the binary assembly has effectively isolated each individual PbSe hexamer enabling controlled fusion of the particles in the box.

Beyond insights into the local structural transformation of the hexamer, *in situ* GISAXS also informs the evolution of the BNSL structure during annealing. A loss of long-range orientational ordering of the superlattice cell would be evident from a broadening of the scattering peaks into sharp rings in the 2D pattern; this trend is not

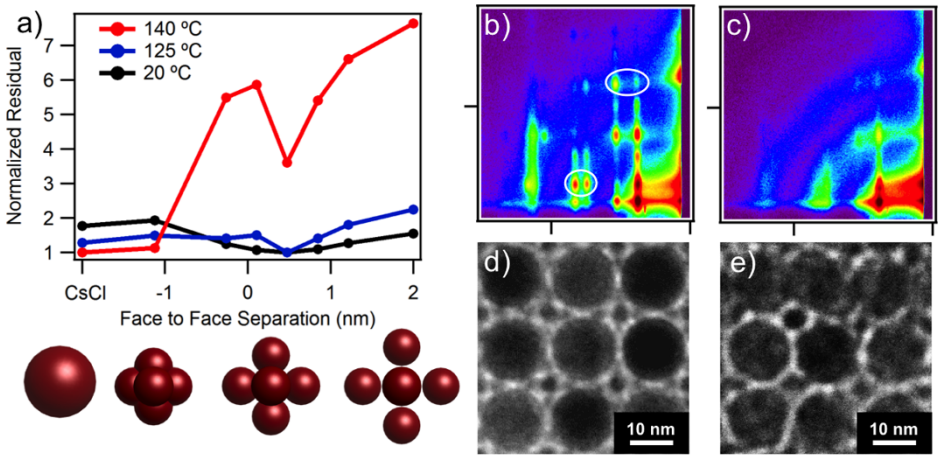

Figure 4 | X-ray Scattering and Transmission Electron Microscopy indicate selective fusion of PbSe NCs. (a) Residuals from comparing calculated to observed scattering patterns as the annealing temperature is increased. The residuals have been normalized relative to the best-fit pattern. Below: Models of the simulated PbSe configuration for a CsCl structure, −1.2 nm, 0.5 nm, and 2 nm face to face spacing, respectively. (b, c) GISAXS patterns at 30° and 130°C, respectively, white ovals indicate the scattering peaks whose relative intensities change during the annealing. Tick marks indicate 1 nm^{-1}. (d, e) TEM images of BNSL before and after annealing, showing fusion of the PbSe particles in the hexamer.

observed during the thermal annealing. Instead we find that the sharp peaks indicative of long-range order become weaker and the diffuse rings corresponding to the form factor of uncorrelated NC become stronger. Furthermore, some broadening of the Bragg reflections indicates reduced average size of the superlattice grains. This can be discerned from the scattering patterns in Figure 4 as well as the video in the supplementary information. To clearly illustrate main trends, we azimuthally integrated the 2D scattering patterns in 1D plots analogous to powder patterns in Figure 5a. The resulting 1D plots reveal the transition from sharp peaks to rounded wider peak occurs first at higher q values followed by a similar transition at progressively smaller q values as the temperature is increased.

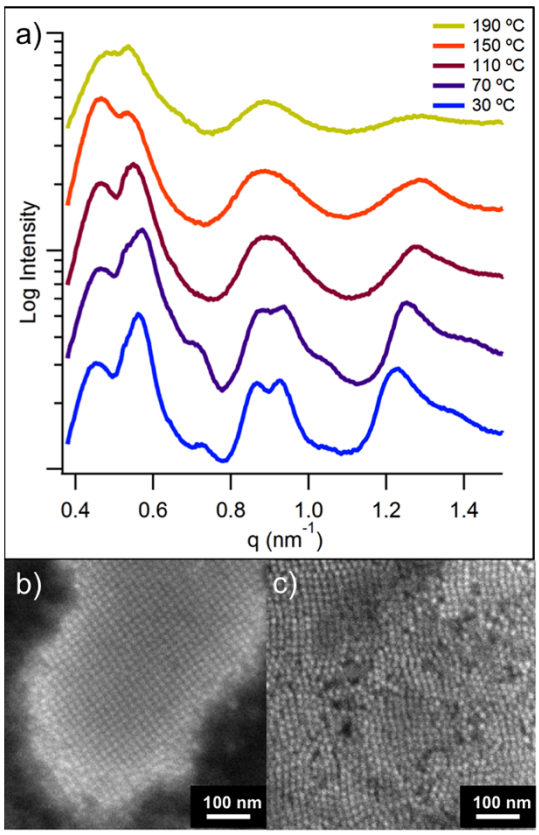

Figure 5 | Loss of film order during thermal annealing. (a) Azimuthal integrations of the scattering patterns as annealing temperature increases. (b, c) SEM images before and after annealing to 190°C, respectively.

This structural evolution in response to thermal annealing is accounted for by the Debye-Waller factor included in the scattering simulation and fitting[20]. As the root-mean-squared displacement of particles from their average positions increases, the intensity of the structure factor is reduced and the intensity of the form factor is increased. This effect is greater at higher q values, and so higher order peaks disappear first. The calculated Debye-Waller factor contains both static and dynamic deviations of both the PbSe and Fe_2O_3 NCs from their ideal lattice sites and we did not attempt to separate these contributions. SEM images after annealing indicate a large static disorder in Fe_2O_3 NCs – consistent with the increase in Debye-Waller factor found by fitting the scattering patterns.

The fusion of six PbSe NCs in the hexamer into one larger particle has significant implications on the structure of the BNSL. This process transforms the BSNL structure from AB_6 into an AB′ (*i.e.* CsCl, *Pm3m*) superlattice. Interestingly, based on the ratio of particle diameters, a single hard sphere of diameter 7.6 nm PbSe NC (resulting from complete fusion of the hexamer) surrounded by 13.4 nm Fe_2O_3 NCs would be more stable in the a NaCl (*i.e.*, *Fm3m*) superlattice structure with 6-fold coordination. A topotactic relation between the *Fm3m* and *Pm3m* structures is expected since the primitive cubic and face-centered cubic lattices of the Fe_2O_3 NCs are related through the primitive rhombohedron of the face-centered cubic lattice. The *Fm3m*-to-*Pm3m* transformation has been studied in atomic crystals, *e.g.*, alkali and ammonium halides[31–33]. To the best of our knowledge, these transformations have not been observed in NC superlattices. The X-ray scattering and SEM data in Figure 5 illustrate a disordering of the superlattice, however further work is required to better understand the binary superlattice symmetry transformation and to decisively delineate this transformation from other changes such as desorption and evaporation of the ligands and fusion of neighboring NCs.

Laser Annealing of BNSLs. Thermal annealing experiments hint towards the existence of an intermediate state involving partial fusion of the PbSe NC that is not observed by GISAXS. To decouple the kinetic and thermodynamic aspects of particle fusion, we used Laser Spike Annealing (LSA) to reduce the characteristic time scale of heating to 1 ms rather than minutes[34]. Given the limited diffusion of the particles in the hexamer during the short-time

heating pulse, we hypothesized the possibility of kinetically trapping the hexamer structure evolution in an intermediate state before it proceeds to the final state observed in the hot plate annealing experiments.

Our analysis of the GISAXS patterns of the laser annealed samples indicates that the assemblies maintain their order better compared to the *in situ* thermally annealed assemblies. Moreover, the plot of Debye-Waller factor vs annealing temperature in Figure 6a indicates that the laser annealed films maintain a higher degree of ordering compared to films treated at similar temperatures with conventional annealing. Importantly, our analysis of simulated and experimental scattering intensities of laser annealed BNSLs summarized in Figure 6c suggests that the NCs in the hexamer are only partially fused when they heated up to temperatures of 197 and 263°C for short periods of time. Reducing the duration of the high-temperature pulse limits the atomic diffusion and traps the neck formation in the hexamer in a transition state. Further investigation of LSA of NC assemblies may facilitate precise control over the level of fusion occurring in a NC film, allowing for creation of 'confined-but-connected' NC solids through physical processing.

Conclusion

We have used the self-assembly of BNSLs to confine PbSe hexamers into a nanoreactor, enabling the study of interactions among a specifically programmable number of NCs. The periodic nature of the BNSL nanoreactor allows for analysis via GISAXS resulting in structural information averaged over as many as 10^{10} unit cells. Molecular modeling showed that the shape of the NCs had to be close to that of truncated octahedra; cube-octahedra and truncated cube shapes were shown to be incapable of forming a hexamer without fusing. Steered Molecular Dynamics simulations showed that the experimentally observed distance of 4.7 nm between NCs is only consistent with a low ligand density of about one molecule per nm^2. The oleic acid ligands have to interdigitate strongly, in order to accommodate the closely spaced NCs. Using the enhanced thermal stability of BNSLs we observed the fusion of six separate NCs into a single hexamer via detailed analysis of *in situ* scattering patterns. Non-equilibrium processing via LSA enables suppression of the order-disorder transition enabling higher temperature processing without disrupting the BNSL order. Both isolating particles into nanosized volumes via self-assembly of BNSLs and subsequent fast laser processing show promise to create novel designer materials that cannot be obtained by self-assembly alone.

Methods

Materials. Lead oxide (99.99%) selenium (99.999%, powder), trioctlyphosphine (90%, technical grade), oleic acid (OA 70%, technical grade), 1-octadecene (ODE 90%) diphenylphosphine (98%), Iron Pentacarbonyl (99.99%), trioctylamine (98%), trimethylamine N-oxide (98%), toluene (%) and tetrachloroethlyene (99%)were all purchased from Sigma Aldrich and used without further purification.

NC Synthesis. PbSe NCs were synthesized using a procedure adapted from Yu *et al*[35]. In a typical synthesis 0.88 g PbO was mixed with 10.8 g of 1-octadecene and 2.76 g oleic acid in a three- neck flask under nitrogen flow and heated to 150°C for 1 hour until all of the PbO had dissolved. 90 µl diphenylphosphine was mixed with 12 ml of 1 M selenium in trioctylphosphine and quickly injected into the three-neck flask. The mixture was heated back up to 135°C and allowed to grow for 3 minutes until it was quenched. The NCs were isolated from the reaction product by washing three times using hexane/ethanol as the solvent/antisolvent pair.

Fe_2O_3 NCs were synthesized using a procedure adapted from Hyeon *et al*[36]. In a typical synthesis 0.65 g oleic acid was mixed with 10 ml of trioctlyamine and heated under vacuum at 250°C for 1 hour. 0.2 ml of iron pentacarbonyl was injected into the solution and allowed to react for 20 minutes at 250°C before being heated to 320°C for an hour in order to form monodisperse iron NCs. The reaction was then cooled to room temperature without quenching and 0.17 g trimethylamine N-oxide was added to the reaction mixture and subsequently heated to 130 C for 1 hour to oxidize the NCs. The NCs were isolated from the reaction product by washing, as described above.

Assembly of Binary NC Superlattices. Superlattices were assembled via controlled evaporation of a solution of half toluene half tetracholorethylene containing both Fe_2O_3 and PbSe NCs. The concentration of NCs in the solution was 1 mg/ml. Appropriate amounts of NCs were added to target a 6 : 1 PbSe: Fe_2O_3 ratio. Particle concentrations were estimated following the procedure outlined in Smith et al[37]. A substrate, either a TEM grid or cleaned Si wafer fragment, and a volume of solution sufficient to cover the substrate was tilted at a 45° angle and placed in a vacuum oven at 50°C and 30 kPa and left to dry overnight.

Sample Characterization. Transmission Electron Microscopy was performed on a FEI Tecnai T12 operating at 120 kV. Scanning Electron Microscopy was performed on a LEO 1550 FESEM. Optical Microscopy was performed with an Olympus BH-2 operating in bright field mode. All images were acquired digitally.

GISAXS was performed at the D1 beam line of the Cornell High Energy Synchrotron Source (CHESS) using monochromatic radiation of wavelength 1.161 Å and a bandwidth $\Delta\lambda/\lambda = 1.5\%$.The X-ray beam was produced by a hardbent dipole magnet of the Cornell storage ring and monochromatized with Mo:B_4C synthetic multilayers with a period of 30 Å. GISAXS images were collected by a MedOptics fiber coupled CCD camera with a pixel size of 46.9 µm by 46.9 µm and a total of 1024 by 1024 pixels with 14 bit dynamical range per pixel. The sample to detector distance was 930 mm, as calibrated by a silver behenate powder standard. Images were dark current corrected, distortion corrected, and flat field corrected by the acquisition software. The incident angle of the X-ray beam was between .2° and .4°, with most data shown collected at .25°. Scattering images were calibrated and integrated using the Fit2D software[38]. GISAXS peaks were indexed using our in-house software[39].

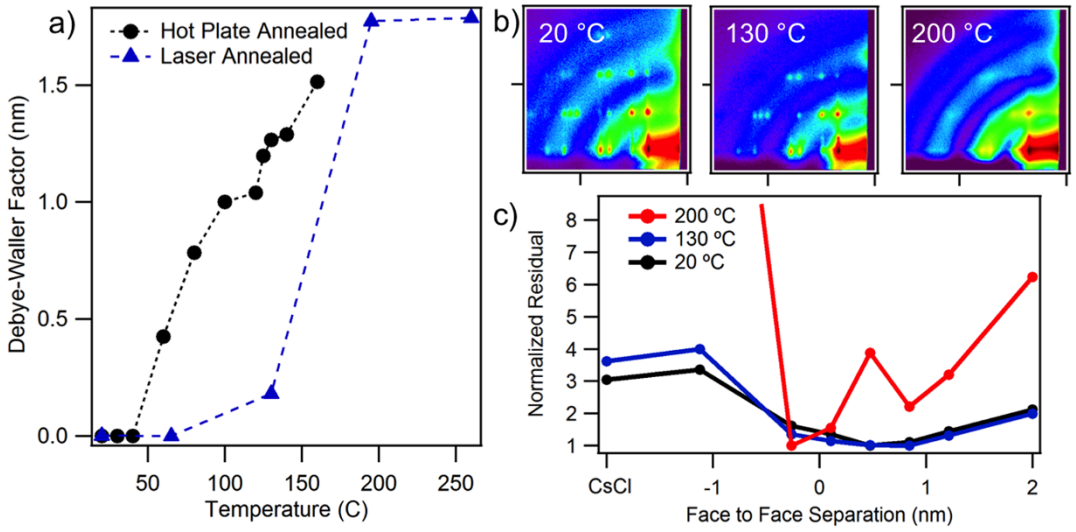

Figure 6 | Laser Spike Annealing of BNSLs. (a) Debye-Waller factor from the best-fit scattering patterns. The dotted lines serve as a guide to the eye and do not represent any theoretical fit to the data. (b) GISAXS patterns for laser annealed samples showing retention of peaks at higher temperatures compared to hot plate annealing. (c) Residuals from comparison of simulated to experimental scattering intensities indicate incomplete fusion.

Sample Annealing. *In situ* annealing was performed by placing a GISAXS sample onto a heating stage custom built at the D1 station at CHESS. The stage was heated by two heating cartridges, inserted into holes in the aluminum stage. The heating cartridges were connected to a variac to control the power input, and the temperature was monitored by a thermocouple placed between the heating cartridges. GISAXS samples were heated from 30°C to 200°C at a rate of 2°C/min.

Laser Spike Annealing was performed by scanning a continuous wave CO_2 laser (λ = 10.6 μm) across a sample. The radiation is absorbed by the highly doped Si substrate, which conductively heats the BNSL film. The laser was focused to a beam with a Gaussian full width half maximum (FWHW) of 100 μm in the direction of a scan and 500 μm in the lateral direction. Scans were performed at a velocity of 100 mm/s corresponding to a dwell time of 1 ms. Scans overlapped with a portion of the previous scan to ensure film uniformity.

1. Baxter, J. *et al.* Nanoscale design to enable the revolution in renewable energy. *Energy Environ. Sci.* **2**, 559–588, doi: 10.1039/B821698C (2009).
2. Milliron, D. J., Gur, I. & Alivisatos, A. P. Hybrid Organic–Nanocrystal Solar Cells. *MRS Bulletin* **30**, 41–44 doi: 10.1557/mrs2005.8 (2005).
3. Nozik, A. J. *et al.* Semiconductor Quantum Dots and Quantum Dot Arrays and Applications of Multiple Exciton Generation to Third-Generation Photovoltaic Solar Cells. *Chem. Rev.* **110**, 6873–6890, doi: 10.1021/cr900289f (2010).
4. Zhou, Z.-Y., Tian, N., Li, J.-T., Broadwell, I. & Sun, S.-G. Nanomaterials of high surface energy with exceptional properties in catalysis and energy storage. *Chem. Soc. Rev.* **40**, 4167–4185, doi: 10.1039/C0CS00176G (2011).
5. Crabtree, G. W. & Sarrao, J. L. Opportunities for mesoscale science. *MRS Bulletin* **37**, 1079–1088, doi: 10.1557/mrs.2012.274 (2012).
6. Bruce, P. G., Scrosati, B. & Tarascon, J.-M. Nanomaterials for Rechargeable Lithium Batteries. *Angew. Chem. Int. Ed.* **47**, 2930–2946, doi: 10.1002/anie.200702505 (2008).
7. Vineis, C. J. *et al.* Nanostructured Thermoelectrics: Big Efficiency Gains from Small Features. *Adv. Mat.* **22**, 3970–3980 doi: 10.1002/adma.20100839 (2010).
8. Shevchenko, E. V., Talapin, D. V., Kotov, N. A., O'Brien, S. & Murray, C. B. Structural diversity in binary nanoparticle superlattices. *Nature* **439**, 55–59 doi: 10.1038/nature04414 (2006).
9. Dong, A., Chen, J., Vora, P., Kikkawa, J. & Murray, C. Binary nanocrystal superlattice membranes self-assembled at the liquid-air interface. *Nature* doi: 10.1038/nature09188 (2010).
10. Kang, Y. *et al.* Engineering Catalytic Contacts and Thermal Stability: Gold/Iron Oxide Binary Nanocrystal Superlattices for CO Oxidation. *J. Am. Chem. Soc.* **135**, 1499–1505, doi: 10.1021/ja310427u (2013).
11. Urban, J. J., Talapin, D. V., Shevchenko, E. V., Kagan, C. R. & Murray, C. B. Synergism in binary nanocrystal superlattices leads to enhanced p-type conductivity in self-assembled PbTe/Ag2Te thin films. *Nat. Mater.* **6**, 115–121 doi: 10.1038/nmat1826 (2007).
12. Ben-Simon, A., Eshet, H. & Rabani, E. On the Phase Behavior of Binary Mixtures of Nanoparticles. *ACS Nano* **7**, 978–986, doi: 10.1021/nn302712h (2013).
13. Kaushik, A. P. & Clancy, P. Solvent-driven symmetry of self-assembled nanocrystal superlattices–A computational study. *J. Comput. Chem.* **34**, 523–532, doi: 10.1002/jcc.23152 (2013).
14. Kovalenko, M. V. *et al.* Colloidal Nanocrystals with Molecular Metal Chalcogenide Surface Ligands. *Science* **324**, 1417–1420 doi: 10.1126/science.1170524 (2009).
15. Wang, Z. *et al.* Deviatoric Stress Driven Formation of Large Single-Crystal PbS Nanosheet from Nanoparticles and in Situ Monitoring of Oriented Attachment. *J. Am. Chem. Soc.* **133**, 14484–14487, doi: 10.1021/ja204310b (2011).
16. Goodfellow, B. W., Patel, R. N., Panthani, M. G., Smilgies, D. & Korgel, B. A. Melting and Sintering of a Body-Centered Cubic Superlattice of PbSe Nanocrystals Followed by Small Angle X-ray Scattering. *J. Phys. Chem. C* **115**, 6397–6404 doi: 10.1021/jp2004908 (2011).
17. Goodfellow, B. W. *et al.* Ordered Structure Rearrangements in Heated Gold Nanocrystal Superlattices. *Nano Lett.* **13**, 5710–5714, doi: 10.1021/nl403458q (2013).
18. Smilgies, D.-M. Scherrer grain-size analysis adapted to grazing-incidence scattering with area detectors. *J. Appl. Crystallogr.* **42**, 1030–1034, doi: 10.1107/S0021889809040126 (2009).
19. Smilgies, D.-M., Heitsch, A. T. & Korgel, B. A. Stacking of Hexagonal Nanocrystal Layers during Langmuir–Blodgett Deposition. *J. Phys. Chem. B* **116**, 6017–6026, doi: 10.1021/jp3015436 (2012).
20. Heitsch, A. T., Patel, R. N., Goodfellow, B. W., Smilgies, D.-M. & Korgel, B. A. GISAXS Characterization of Order in Hexagonal Monolayers of FePt Nanocrystals. *J. Phys. Chem. C* **114**, 14427–14432, doi: 10.1021/jp1047979 (2010).
21. Glatter, O. & Kratky, O. *Small angle X-ray scattering.* Vol. 102 (Academic press London, 1982).
22. Förster, S. *et al.* Scattering Curves of Ordered Mesoscopic Materials. *J. Phys. Chem. B* **109**, 1347–1360, doi: 10.1021/jp0467494 (2005).
23. Hanrath, T., Choi, J. J. & Smilgies, D.-M. Structure/Processing Relationships of Highly Ordered Lead Salt Nanocrystal Superlattices. *ACS Nano* **3**, 2975–2988, doi: 10.1021/nn901008r (2009).
24. Paul, W., Yoon, D. Y. & Smith, G. D. An optimized united atom model for simulations of polymethylene melts. *J. Chem. Phys.* **103**, 1702–1709, doi: 10.1063/1.469740 (1995).
25. Tang, J. *et al.* Colloidal-quantum-dot photovoltaics using atomic-ligand passivation. *Nat Mater* **10**, 765–771, doi: 10.1038/nmat3118 (2011).
26. Talapin, D. V. & Murray, C. B. PbSe Nanocrystal Solids for n- and p-Channel Thin Film Field-Effect Transistors. *Science* **310**, 86–89, doi: 10.1126/science.1116703 (2005).
27. Baumgardner, W. J. *et al.* Pulsed Laser Annealing of Thin Films of Self-Assembled Nanocrystals. *ACS Nano* **5**, 7010–7019, doi: 10.1021/nn201588p (2011).
28. Rickey, K. M. *et al.* Effects of rapid thermal processing and pulse-laser sintering on CdTe nanofilms for photovoltaic applications. *SPIE Nano. Eng.* 846505 doi: 10.1117/12.929965 (2012).
29. van Huis, M. A. *et al.* Low-Temperature Nanocrystal Unification through Rotations and Relaxations Probed by in Situ Transmission Electron Microscopy. *Nano Lett.* **8**, 3959–3963, doi: 10.1021/nl8024467 (2008).
30. Schapotschnikow, P., Huis, M. A., Zandbergen, H. W., Vanmaekelbergh, D. & Vlugt, T. J. Morphological Transformations and Fusion of PbSe Nanocrystals Studied Using Atomistic Simulations. *Nano Lett.* **10**, 3966–3971 (2010).
31. Buerger, M. Phase transformations in solids. *John Wiley*, 183 (1951).
32. Kennedy, S. W., Patterson, J. H., Chaplin, R. P. & Mackay, A. L. The transformation of CsCl type ⇋ NaCl type. Part II: Orientation relations in phase transformations CsCl type → NaCl type in ammonium halides. *J.Solid State Chem.* **10**, 102–107, doi: 10.1016/0022-4596(74)90014-0 (1974).
33. Fraser, W. L. & Kennedy, S. W. The transformation Fm3m to Pm3m in ammonium bromide. *Acta Crystallogr. Sect. B* **28**, 3101, doi: 10.1107/S0567740872007514 (1972).
34. Iyengar, K., Jung, B., Willemann, M., Clancy, P. & Thompson, M. O. Experimental determination of thermal profiles during laser spike annealing with quantitative comparison to 3-dimensional simulations. *Appl. Phys. Lett.* **100**, doi: 10.1063/1.4717745 (2012).
35. Yu, W. W., Falkner, J. C., Shih, B. S. & Colvin, V. L. Preparation and Characterization of Monodisperse PbSe Semiconductor Nanocrystals in a Noncoordinating Solvent. *Chem. Mater.* **16**, 3318–3322, doi: 10.1021/cm049476y (2004).
36. Hyeon, T., Lee, S. S., Park, J., Chung, Y. & Na, H. B. Synthesis of Highly Crystalline and Monodisperse Maghemite Nanocrystallites without a Size-Selection Process. *J. Am. Chem. Soc.* **123**, 12798–12801, doi: 10.1021/ja016812s (2001).
37. Smith, D. K., Goodfellow, B., Smilgies, D. & Korgel, B. A. Self-Assembled Simple Hexagonal AB Binary Nanocrystal Superlattices: SEM, GISAXS, and Defects. *J. Am. Chem. Soc.* **131**, 3281–3290 doi: 10.1021/ja8085438 (2009).
38. Hammersley, A. FIT2D: an introduction and overview. *European Synchrotron Radiation Facility Internal Report ESRF97HA02T* (1997) (Date of access: 04/30/2014) (available at: http://www.csb.yale.edu/userguides/datamanip/fit2d/fit2d_ref.pdf).
39. Smilgies, D.-M. & Blasini, D. R. Indexation scheme for oriented molecular thin films studied with grazing-incidence reciprocal-space mapping. *J. Appl. Crystallogr.* **40**, 716–718 doi: 10.1107/S0021889807023382 (2007).

Acknowledgments

The authors thank Professor Michael O. Thompson for assistance with the laser spike annealing. BT acknowledges the financial support of NSF GK-12 award DGE-1044413 "Grass Roots: Advancing education in renewable energy and cleaner fuels through collaborative graduate fellow-teacher/grade-school student interactions." BL acknowledges the support of the Semiconductor Research Corporation, Task 2272.001. This work made use of the Cornell Center for Materials Research Shared Facilities which are supported through the NSF MRSEC program (DMR-1120296). TH acknowledges support from the NSF-DMR (1056943). X-ray scattering experiments were conducted at the Cornell High Energy Synchrotron Source (CHESS), which is supported by the National Science Foundation and the National Institutes of Health/National Institute of General Medical Sciences under NSF award DMR-0936384 and DMR-1332208.

Author contributions

B.T. designed and performed experiments. B.T. and D.S. analyzed the data. B.L. and P.C. performed the molecular dynamics simulations. B.T. and T.H. wrote the main manuscript and prepared figures. T.H. developed the initial concept and supervised the study.

Additional information

Supplementary information accompanies this paper at http://www.nature.com/scientificreports

Competing financial interests: The authors declare no competing financial interests.

How to cite this article: Treml, B.E., Lukose, B., Clancy, P., Smilgies, D.-M. & Hanrath, T. Connecting the Particles in the Box - Controlled Fusion of Hexamer Nanocrystal Clusters within an AB_6 Binary Nanocrystal Superlattice. *Sci. Rep.* **4**, 6731; DOI:10.1038/srep06731 (2014).